

Low-energy electron thermal diffuse scattering from Al(111) individually resolved in energy and momentum

V. Zielasek, A. Büssenschütt, and M. Henzler

Universität Hannover, Institut für Festkörperphysik, Appelstrasse 2, D-30 167 Hannover, Germany

(Received 5 June 1996)

A low-energy-electron-diffraction (LEED) system which provides high resolution in energy and momentum simultaneously has been used to measure the intensity and the angular distribution of the thermal diffuse scattering (TDS) of Al(111) within the first surface Brillouin zone. The kinematic scattering theory is shown to provide a good description of the experimental results. Especially the one-phonon scattering is seen to decrease radially with distance $|\mathbf{K}_\parallel|$ from the (00)-Bragg rod at about $1/|\mathbf{K}_\parallel|$. Here the pioneering experiments of about 30 years ago are expanded and one-phonon, multiple-phonon, and elastic scattering throughout the Brillouin zone are separated in the experimental data with the help of energy resolution. The discussion shows to what extent TDS is affecting the defect analysis using a spot profile analysis of LEED without an energy resolution. [S0163-1829(97)03408-5]

I. INTRODUCTION

A sharp diffraction spot in a low-energy-electron-diffraction (LEED) experiment reveals a long range periodicity of a solid, in the same way information about imperfections is derived from the broadening of the spots and from an elastic background intensity. The spot profile analysis of high resolution LEED (SPA-LEED) is a highly developed tool to study all kinds of surface defects. The advantage over imaging techniques is the quantitative defect evaluation. Since the kinematic approximation provides very detailed results, the procedures to extract data on the average density of defects and their distribution from spot profiles are easy to use.¹⁻³

The accuracy of the analysis with usual instrumentation is limited by the inelastic thermal diffuse scattering (TDS). Since the suppressor of a conventional LEED or SPA-LEED instrument does not cut off phonon scattering, the contribution of the TDS to spot profile and background intensity has widely been assumed to be a constant or even the only contribution to the background or it has been just neglected.

Our energy loss spectroscopy-LEED (ELS-LEED) (Ref. 4) provides high resolution in energy and momentum simultaneously allowing us not only to separate the TDS from elastic scattering due to surface defects directly in the experiment. We also may study the thermal diffuse scattering with a higher angular resolution than with the available instrumentation designed only for high energy resolution.⁵ We present our results for the intensity and the angular distribution within the first surface Brillouin zone (SBZ) of one-phonon and multiple-phonon scattering of low-energy electrons at Al(111) and refer them to theoretical predictions within the kinematic approximation.

About 30 years ago Webb and co-workers have measured spot profiles including TDS with lower angular resolution and with integration over the full phonon energy range.⁶⁻⁸ Their far reaching conclusions are now substantiated and clarified, because an experimental separation of elastic, one-phonon, and multiple-phonon scattering is realized in the present experiments.

II. THEORETICAL PREDICTIONS

It has been shown that within the validity range of the kinematic approximation the diffracted intensity may be described, as if it would come entirely from scattering in the surface layer.¹ If the thermal displacement $\mathbf{u}_n(t)$ of atom n from its equilibrium site \mathbf{r}_n is small with respect to the next neighbor distance, the intensity scattered from a monatomic lattice may be described within the kinematic approximation as:⁹

$$I(\mathbf{K}) = |f_0|^2 \sum_n \sum_m e^{i\mathbf{K}(\mathbf{r}_n - \mathbf{r}_m)} e^{-\langle (\mathbf{K}\mathbf{u}_n)^2 \rangle} \left(1 + \langle (\mathbf{K}\mathbf{u}_n)(\mathbf{K}\mathbf{u}_m) \rangle + \frac{\langle (\mathbf{K}\mathbf{u}_n)(\mathbf{K}\mathbf{u}_m) \rangle^2}{2!} + \dots \right). \quad (1)$$

Here \mathbf{K} is the scattering vector, f_0 is the atomic scattering factor, and $\langle \rangle$ stands for the thermal average. While the first term in the brackets denotes the elastic scattering the TDS comprises the second term corresponding to single-phonon scattering and all remaining terms corresponding to multiple-phonon scattering.⁸

Integration over the entire surface Brillouin zone yields with I_1 and I_0 (single-phonon and elastic scattering, respectively):⁸

$$I_1 = 2M_S I_0. \quad (2)$$

$2M_S$ is the exponent of the surface Debye-Waller factor. In the high temperature limit it is proportional to temperature and to the incident electron energy.

The evaluation of the single-phonon scattering has been reported in Ref. 10 for all kinds of vibrational modes of a free surface approximating the crystal as an isotropic elastic continuum. The prediction for the distribution of the one-phonon scattering within the first surface Brillouin zone is for surface waves as well as for bulk related modes (\sim denotes proportionality and \otimes denotes convolution):

$$I_1(\mathbf{K}_{\parallel}) \sim \frac{1}{K_{\parallel}} \otimes I^*(\mathbf{K}_{\parallel}). \quad (3)$$

$I^*(\mathbf{K}_{\parallel})$ is the diffracted intensity as expected from a rigid lattice.

Validity is claimed only in the vicinity of the (00) spot due to the approximations. It is assumed that the Rayleigh mode exhibits a linear dispersion. For $K_{\perp} \gg K_{\parallel}$ it is shown that surface waves and bulk related modes (combination and mixed modes) should contribute by about the same amount to inelastic scattering.

For bulk related modes a simple derivation is sketched in Ref. 7 where it is assumed that the thermal motion of the surface atoms can be described by a Debye spectrum of the bulk. The result approaches (3) in the vicinity of the (00)-Bragg rod:

$$I_2(\mathbf{K}_{\parallel}) \sim \frac{1}{K_{\parallel}} \arctan\left(\frac{\pi}{K_{\parallel}d}\right) \otimes I^*(\mathbf{K}_{\parallel}). \quad (4)$$

Those equations will be used for comparison with the experimental results.

III. EXPERIMENT

The Al specimen was cut within 0.1° of the (111) orientation from a single crystal boule of high purity (99.999%) by means of spark erosion. It was mechanically polished and finally electropolished in a mixture of perchloric acid (0.05% vol.) and ethyl alcohol. *In situ* cleaning was performed by cycles of argon ion bombardment of the heated specimen (temperature 550 K) for several hours and annealing up to 900 K. The final Auger spectrum did not show any impurities (contamination with C, O less than 0.1%).

The temperature was measured using a NiCr-Ni thermocouple fixed in a groove in the edge of the specimen. The sample was heated by radiation from a tungsten filament and cooled with LN_2 .

The ELS-LEED instrument may be considered either as a high-resolution electron-energy-loss spectrometer (HREELS) with high momentum resolution or as a HRLEED system with high energy resolution. The electrostatic deflection unit ("octopole") of a SPA-LEED system allows us to scan diffraction patterns keeping the positions of the electron gun, the specimen and the detector fixed. The electron gun and detector are equipped with one 127° HREELS cylindrical deflector each as a monochromator and energy analyzer, respectively.

For incident energies of 3–300 eV a momentum resolution of 0.042 nm^{-1} [which corresponds to 0.15% of a vector of the reciprocal lattice of the Al(111) surface] in combination with an energy resolution of 4–8 meV is achieved. Details of the instrument and the ultrahigh vacuum system can be found elsewhere.⁴

IV. RESULTS AND DISCUSSION

The first part of this section describes the determination of the TDS from measurements with high energy resolution, the second part shows an alternative measurement of TDS with low energy resolution simulating the results as obtained with a conventional LEED or SPA-LEED instrument.

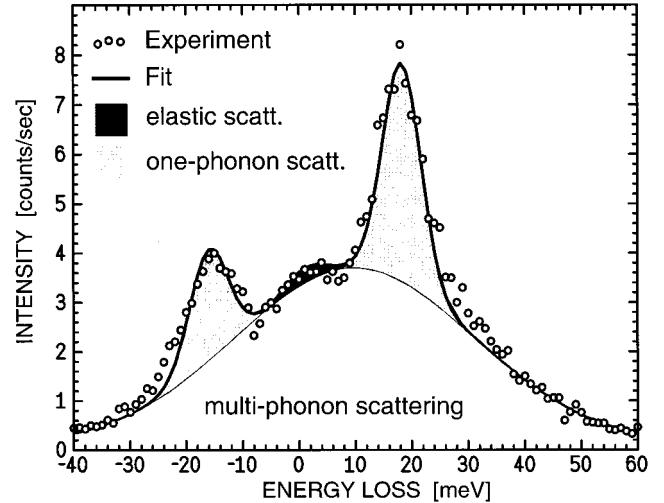


FIG. 1. Energy loss spectrum at the \bar{M} point for incident electron energy 61.5 eV at room temperature. Measuring points are shown as open circles. As a result of the fitting procedure described in the text, the light gray areas denote scattering due to the annihilation and creation of a single Rayleigh phonon, the small dark gray area in their midst denotes elastic scattering due to surface defects and the solid line beneath shows the multiple-phonon background.

A. Experiments with high energy resolution

The thermal diffuse scattering has been evaluated from electron energy loss spectra recorded at various points of the surface Brillouin zone. The energy resolution measured in specular geometry was 8 meV fullwidth at half maximum (FWHM). The spectrum at the \bar{M} -point recorded at room temperature with 61.5 eV incident electron energy is shown in Fig. 1. Loss and gain at $|\Delta E| \approx 17 \text{ meV}$ are due to creation and annihilation of the Rayleigh phonon. The dispersion is well known from helium atom scattering (HAS) experiments¹² and has been reproduced in our experiments within the instrumental resolution.

The spectrum is fitted using a Gaussian shaped curve with variable intensity and FWHM denoting the multiple scattering background and three peaks with the shape of the specular EELS which stand for gain and loss due to the Rayleigh mode scattering (light gray areas) and elastic scattering due to surface defects (dark gray area). The center of the multiple-phonon scattering is shifted due to the higher probability for energy loss.

Figure 2 shows several spectra along the line $\bar{\Gamma}-\bar{M}$ (0% SBZ is at $\bar{\Gamma}$, 50% SBZ is at \bar{M}). The spectra have been fitted according to Fig. 1 using a least square fitting routine. A prerequisite for a reliable evaluation of the TDS throughout the entire surface Brillouin zone is a fairly low elastic scattering outside the Bragg peaks. For incident energies of 26, 61.5, and 110 eV [corresponding to the (222), (333), and (444) Bragg spot, respectively] atomic steps do not cause broadening of the Bragg peaks since the scattering of adjacent atomic layers interferes constructively (in-phase condition).³ After optimizing *in situ* surface preparation with respect to surface contamination the elastic intensity (the difference between the solid line and measuring points in Fig. 2 and the black area in Fig. 1) is much smaller than the TDS (solid line).

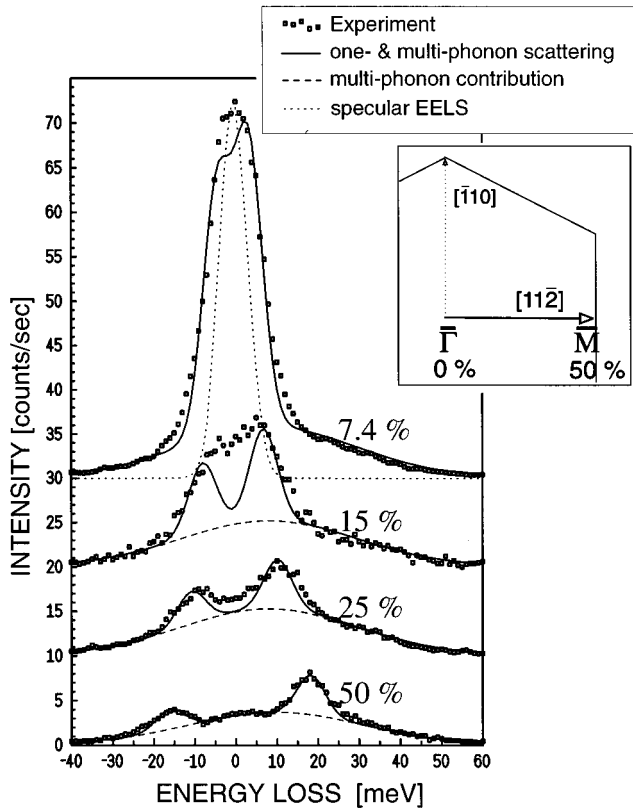


FIG. 2. Energy loss spectra at \bar{M} (50% SBZ) and at 7.4, 15, and 25% SBZ along $\bar{\Gamma}-\bar{M}$. Measuring points are shown as squares, the dashed line reproduces the fitted multiple-phonon losses and the solid line the fit of all losses. The shape of the specular EELS is shown as a dotted line below the spectrum at 7.4% SBZ on a different scale. Otherwise the same conditions as in Fig. 1.

The dotted line in the spectrum at 7.4% SBZ along $\bar{\Gamma}-\bar{M}$ of Fig. 2 denotes the shape of the spectrum measured in specular geometry to show that already the spectrum at 7.4% SBZ is broadened due to single-phonon scattering. The fitting procedure took the energy of the Rayleigh mode for small wave vectors from the HAS results.¹²

The intensities of multiple-phonon (open triangles) and single-phonon scattering (filled triangles) determined from similar spectra measured at 110 eV incident energy along $\bar{\Gamma}-\bar{M}$ are plotted versus the parallel component of the scattering vector in Fig. 3. The multiple-phonon scattering appears nearly constant throughout the entire surface Brillouin zone. The one-phonon scattering is well described as proportional to $1/K_{\parallel}$ (dashed line) for small scattering vectors. For larger scattering vectors the measured one-phonon intensity falls off more rapidly than expected from the $1/K_{\parallel}$ fit. Surprisingly the theoretical prediction from Ref. 7 cited in Eq. (4) (solid line) is a very good approximation even at the SBZ boundary.

The isotropy of the TDS in the first surface Brillouin zone can be seen in Fig. 4, which shows the results of the measurements for an incident energy of 61.5 eV. [The dashed and solid line show the $1/K_{\parallel}$ and the $\arctan(\pi/K_{\parallel}d)/K_{\parallel}$ fit as in Fig. 3]. The triangles, diamonds, and squares denote the experimental results for the one-phonon and the multiple-phonon scattering in the $[11\bar{2}]$, $[\bar{1}12]$, and $[110]$ direction, respectively.

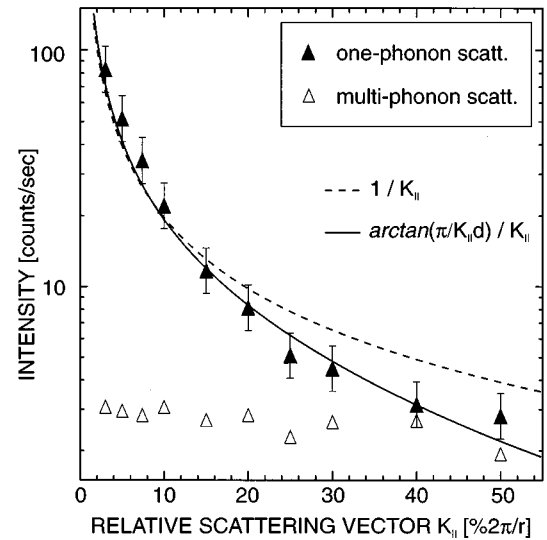


FIG. 3. Intensities for multiple-phonon scattering (open triangles) and one-phonon scattering (filled triangles) evaluated from the energy loss spectra along $\bar{\Gamma}-\bar{M}$ for the incident electron energy 110 eV at room temperature. The dashed line shows a $1/K_{\parallel}$ fit and the solid line an $\arctan(\pi/K_{\parallel}d)/K_{\parallel}$ fit.

The fitting procedures separating elastic scattering and TDS are also useful when the elastic scattering close to the Bragg rods is high due to structural defects. The results of measurements performed at the out-of-phase condition (scattering from adjacent terraces interferes destructively³) and analyzed according to Fig. 3 are shown in Fig. 5. The (00) spot exhibits an elastic shoulder due to atomic steps on the surface (black dots) which is of the same magnitude as the TDS throughout large areas of the SBZ. However the analysis yields the multiple-phonon scattering (crosses) as constant and the one-phonon scattering (triangles) is well de-

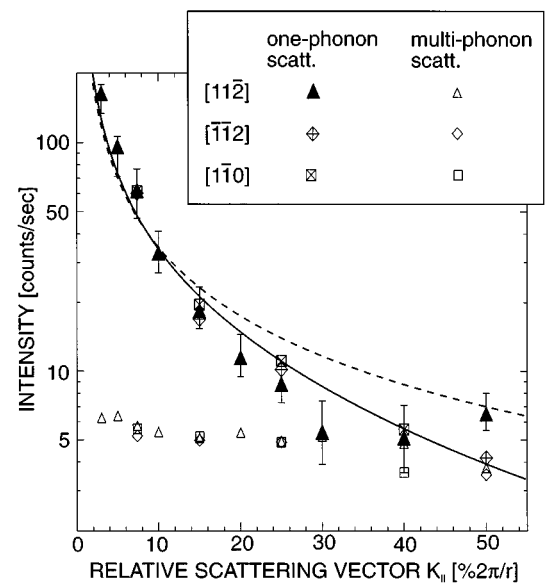


FIG. 4. Results for multiple-phonon and one-phonon scattering intensities evaluated for incident electron energy 61.5 eV at room temperature for scattering vectors in the directions $[11\bar{2}]$, $[\bar{1}12]$, and $[110]$.

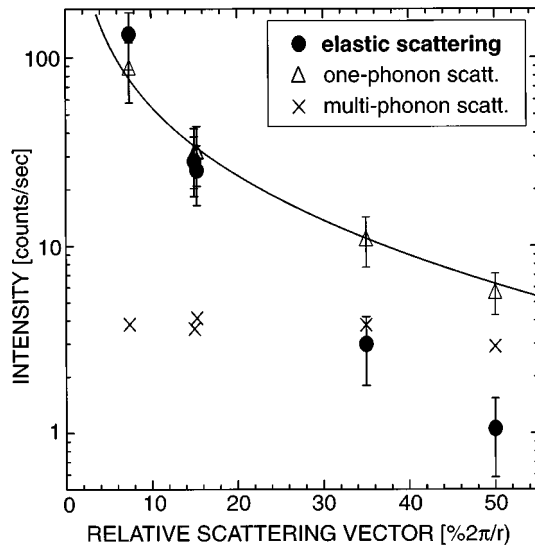


FIG. 5. Same analysis as in Fig. 3 for incident electron energy 42 eV (out-of-phase condition) and temperature $T=400$ K. The (00)-spot is broadened due to destructive interference of scattering from adjacent terraces.

scribed by an $\arctan(\pi/K_{||}d)/K_{||}$ fit (solid line) as it is expected from the measurements at in-phase conditions.

Figure 6 shows our results of similar measurements of the one-phonon scattering for various incident energies (26, 42, 61.5, 110 eV) and various temperatures up to 520 K normalized to their intensity at a distance of 15% SBZ from the (00) spot (large triangle). It is clearly seen that a $1/K_{||}$ fit which is predicted by simple kinematic scattering theory provides a good description for relative scattering vectors up to 10% SBZ.

Deviations from the $1/K_{||}$ dependence for larger wave vectors are expected: Approximating the dispersion as linear is

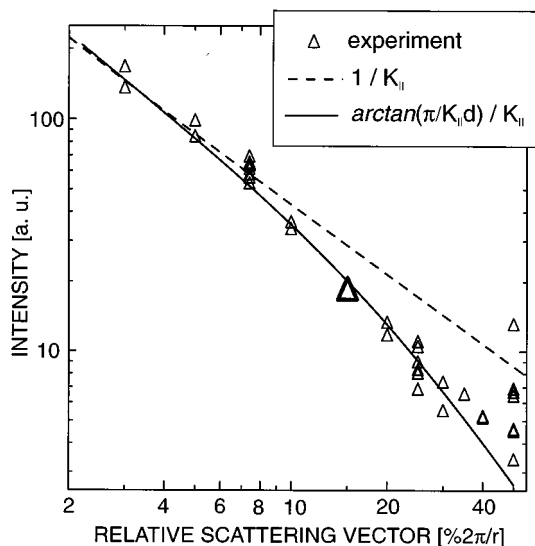


FIG. 6. Intensities for one-phonon scattering from measurements for various incident energies and temperatures normalized to their value at 15% $2\pi/r$ (large triangle). The dashed line shows a $1/K_{||}$ fit and the solid line an $\arctan(\pi/K_{||}d)/K_{||}$ fit.

valid only in the vicinity of the (00)-Bragg rod. Since the slope of the Rayleigh mode dispersion curve decreases near the SBZ boundary the occupation number and the amplitude of the mode are higher than expected which should lead to an increased phonon scattering. On the other hand, the assumption that scattering comes entirely from the topmost surface layer should lead to an overestimation of phonon scattering near the SBZ boundary. Since the vibrational amplitude of surface waves falls off more rapidly into the bulk for larger wave vectors, contributions from deeper layers should enhance the phonon scattering in the vicinity of the (00)-Bragg rod. The limit is the $\arctan(\pi/K_{||}d)/K_{||}$ profile which represents scattering from deep inside the bulk. Further on effects due to multiple scattering might result in an unpredictable cross section for phonon scattering within the kinematic approximation as it has been demonstrated for Ni(100) at the \bar{X} point of the SBZ.¹³ On Al surfaces however the kinematic approximation is expected to provide an appropriate description of LEED experiments,¹¹ which has been shown on Al(110).¹⁴ Empirically we find that $\arctan(\pi/K_{||}d)/K_{||}$ is a universal fit to the single-phonon scattering profile for four different incident electron energies throughout the entire SBZ. This indicates that also the scattering near the zone boundary should not be dominated by dynamical effects. Since the assumptions of Ref. 7 which lead to Eq. (4) do not meet our experimental conditions a modified theoretical approach to surface phonon scattering with validity also for wave vectors near the SBZ boundary is desirable.

B. Experiments with low-energy resolution

As a consequence of the results of the previous section the TDS has to be accounted for in the following manner in any spot profile analysis of LEED without energy resolution: The multiple-phonon scattering can be considered as a constant background. The single-phonon scattering should have a profile according to $\arctan(\pi/K_{||}d)/K_{||}$ convoluted with the elastic profile. Measuring on an ideal crystal this should be a Gaussian shaped curve with its inverse FWHM standing for the instrumental transfer width.

To simulate a conventional SPA-LEED system we set the energy resolution of our instrument to about 60 meV. It is the worst possible resolution with our setup and it is also sufficient to simulate the “quasielastic” scattering of the usual equipment, which does not discriminate elastic scattering, single- and most multiple-phonon scattering due to a resolution of a few eV.

A profile analysis as suggested above is carried out in Fig. 7 for incident electron energy 61.5 eV (in-phase condition). The intensity and FWHM of a Gaussian shaped curve and the intensities of a constant background and a “single-phonon profile” are the free parameters of a least square fitting routine which also performs the convolution of the Gaussian peak with $\arctan(\pi/K_{||}d)/K_{||}$ to simulate the single-phonon scattering during the fitting procedure. The resulting areas of elastic scattering (dark gray), one-phonon scattering (light gray), and multiple-phonon scattering (white area below) are shown in Fig. 7. Their sum fits the experimental profile which is shown with the measuring points perfectly. Thereby the single-phonon profile is measured with a high momentum resolution of 0.5% SBZ (0.14 nm^{-1}) corresponding to the FWHM of the elastic peak.

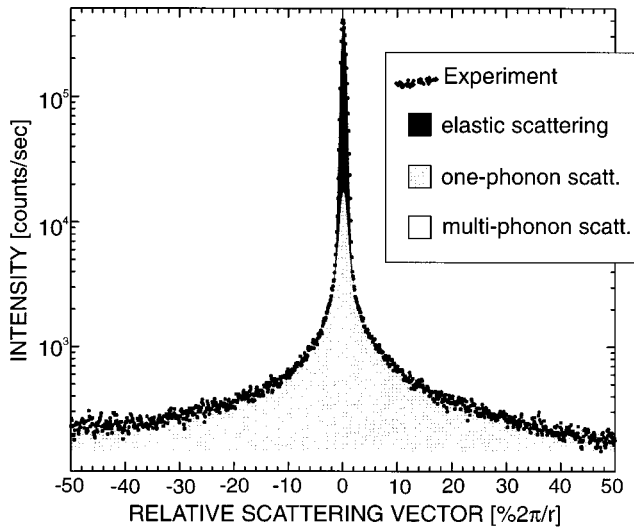


FIG. 7. Profile analysis of the (00) spot considering one-phonon scattering (incident electron energy 61.5 eV, room temperature). Details of the fitting procedure are described in the text.

A conventional spot profile analysis which considers TDS as a constant background throughout the entire surface Brillouin zone would misinterpret the intensity in the wings of the central peak either as due to surface defects or as a result of the instrument. The latter should lead to a modulation of the instrumental transfer function with LEED energy and temperature of the specimen.

Simulated spot profiles comprising the intensities for elastic scattering, one-phonon scattering, and the multiphonon background as expected from the kinematic approximation⁸ are shown in Fig. 8 for various exponents of the Debye-Waller factor. For low temperatures and energies, respectively, the one-phonon wings of the (00) spot (assumed as

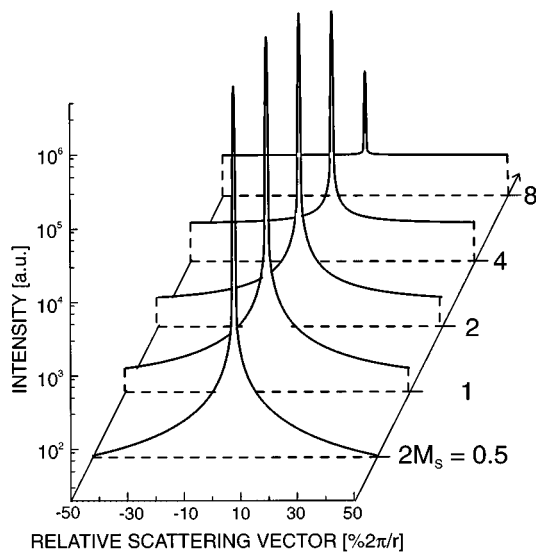


FIG. 8. Simulated spot profiles comprising an elastic Gaussian shaped peak with a fixed FWHM, a one-phonon contribution according to $1/K_{\parallel}$, and a constant multiple-phonon background for various exponents of the Debye-Waller factor ranging from 0.5 to 8. The integral intensities are evaluated from Eq. (2).

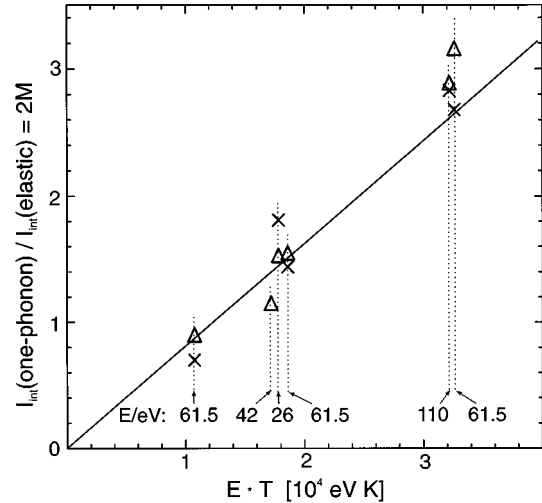


FIG. 9. Relation of the evaluated intensities of one-phonon and elastic scattering versus the exponent of the Debye-Waller factor. Stars show the results of measurements with high-energy resolution, triangles the results of measurements with low-energy resolution. The corresponding incident electron energy is displayed below the symbols. The straight line shows the expected relation for a Debye temperature of 259 K.

Gaussian shaped) are clearly seen in the plot since the one-phonon scattering dominates the multiple-phonon background. The shape of the elastic scattering, however, is practically undistorted over a range of several decades. For high values of $2M_S$ the one-phonon scattering strongly affects the profile after subtraction of the multiple-phonon background since the ratio I_1/I_0 corresponds to $2M_S$, Eq. (2). So the appropriate consideration of the one-phonon scattering within a spot profile analysis without energy resolution is important generally for measurements of low defect densities and especially for high temperature experiments.

The consistency of our analysis within the kinematic approximation is checked with the evaluation of the exponent of the Debye-Waller factor. As usual in LEED experiments we have evaluated $2M_S$ from the exponential decay of the specular intensity with increasing temperature (incident energy $E=26$ eV). $2M_S$ versus ET is shown as a straight line in Fig. 9 and corresponds to a surface Debye temperature Θ_D^S (Ref. 11) of 259 K. The separation of elastic, one-phonon, and multiple-phonon scattering in the experiment, however, provides a direct approach to $2M_S$ by means of I_1/I_0 . Figure 9 shows I_1/I_0 as evaluated individually from the high resolution energy loss spectra (EELS: crosses) and the spot profile analysis with low energy resolution (LEED: triangles) for all our measurements at the given energies and temperatures. The EELS results as well as the results of the spot profile analysis of LEED are in good agreement with $\Theta_D^S=259$ K.

V. CONCLUSIONS

Our instrument shows a reliable separation of elastic, one-phonon, and multiple-phonon scattering. The intensity and angular distribution of the thermal diffuse scattering at Al(111) are in good agreement with the expectations from

the kinematic approach to low-energy electron diffraction. There is no evidence for a modification due to dynamical effects. That might be special for Al surfaces and should be checked with other material.

Already more than 30 years ago Webb *et al.*⁶⁻⁸ investigated the TDS of low-energy electrons at Ag and Ni surfaces and found confirmation for the predictions of the kinematic scattering theory in their results. From today's point of view, however, their LEED system had a poor momentum resolution [FWHM of the (00) spot about a magnitude larger than in our experiments] and it did not provide any energy resolution in the range of phonon energies. Within their resolution in energy and momentum they found a perfect agreement between theory and experiment.

We presented a spot profile analysis for LEED systems without energy resolution which takes into account the broadening of the spot profile by one-phonon scattering. The frequently used approximation to include the one-phonon scattering into the instrumental function (by adding a Lorentzian to the Gaussian function) and subtracting the highest possible constant background intensity (assuming that it is just multiple-phonon scattering) is for aluminum obviously a

good approximation, since the remaining intensity is due to defects. It is questionable if this approximation still holds for higher temperatures. Preliminary experiments with silicon show that there is a strong contribution by point defects to the background. Here an energy resolution is required to account for the high density of point defects. For broad terrace distributions with small terraces again the correct determination of the elastic scattering in the background is important for a precise calculation of the terrace width distribution and the step density.

Many experiments may be done safely with LEED and SPA-LEED without energy resolution. It is, however, obvious, that some experiments should be done with a high resolution instrument like our ELS-LEED to obtain reliable evaluations.

ACKNOWLEDGMENTS

The authors thank H. Froitzheim for many helpful discussions. The investigation has been supported by the Deutsche Forschungsgemeinschaft.

¹M. Henzler, Appl. Phys. A **34**, 205 (1984).

²H. Busch and M. Henzler, Surf. Sci. **167**, 534 (1986).

³J. Wollschläger, J. Falta, and M. Henzler, Appl. Phys. A **50**, 57 (1990).

⁴H. Claus, A. Büssenschütt, and M. Henzler, Rev. Sci. Instrum. **63**, 2195 (1992).

⁵H. Ibach and D.L. Mills, *Electron Energy Loss Spectroscopy and Surface Vibrations* (Academic Press, New York, 1982).

⁶E.R. Jones, J.T. McKinney, and M.B. Webb, Phys. Rev. **151**, 476 (1966).

⁷J.T. McKinney, E.R. Jones, and M.B. Webb, Phys. Rev. **160**, 523 (1967).

⁸R.F. Barnes, M.G. Lagally, and M.B. Webb, Phys. Rev. **171**, 627 (1968).

⁹R.F. Wallis and A.A. Maradudin, Phys. Rev. **148**, 962 (1966).

¹⁰D.L. Huber, Phys. Rev. **153**, 772 (1967).

¹¹M.A. van Hove, W.H. Weinberg, and C.M. Chan, *Low Energy Electron Diffraction*, edited by G. Ertl and R. Gomer, Springer Series in Surface Science Vol. 6 (Springer, Berlin, 1986).

¹²A. Lock, J.P. Toennies, C. Wöll, V. Bortolani, A. Franchini, and G. Santoro, Phys. Rev. B **37**, 7087 (1988).

¹³Mu-Liang Xu, B.M. Hall, S.Y. Tong, M. Rocca, H. Ibach, S. Lehwald, and J.E. Black, Phys. Rev. Lett. **54**, 1171 (1985).

¹⁴H. Göbel and P. von Blanckenhagen, Phys. Rev. B **47**, 2378 (1993).